Virus Research 302 (2021) 198469

Contents lists available at ScienceDirect

Virus Research

journal homepage: www.elsevier.com/locate/virusres

The folate antagonist methotrexate diminishes replication of the coronavirus SARS-CoV-2 and enhances the antiviral efficacy of remdesivir in cell culture models

Kim M. Stegmann [a,1], Antje Dickmanns [a,1], Sabrina Gerber [a], Vella Nikolova [a], Luisa Klemke [a], Valentina Manzini [a], Denise Schlösser [a], Cathrin Bierwirth [a], Julia Freund [a], Maren Sitte [b], Raimond Lugert [c], Gabriela Salinas [b], Toni Luise Meister [d], Stephanie Pfaender [d], Dirk Görlich [e], Bernd Wollnik [f], Uwe Groß [c], Matthias Dobbelstein [a,*]

[a] *Institute of Molecular Oncology, Göttingen Center of Molecular Biosciences (GZMB), University Medical Center Göttingen, Germany*
[b] *NGS Integrative Genomics Core Unit, Institute of Human Genetics, University Medical Center Göttingen, Germany*
[c] *Institute of Medical Microbiology, Göttingen Center of Molecular Biosciences (GZMB), University Medical Center Göttingen, Germany*
[d] *Department of Molecular and Medical Virology, Ruhr University Bochum, Germany*
[e] *Max Planck Institute for Biophysical Chemistry, Göttingen, Germany*
[f] *Institute of Human Genetics, University Medical Center Göttingen, Germany*

ARTICLE INFO

Keywords:
Coronavirus
SARS-CoV-2
COVID-19
Methotrexate
Folic acid
Dihydrofolate reductase
Leucovorin
Folinic acid
Inosine
Remdesivir
Purine synthesis
RNA replication
Spike
Nucleocapsid

ABSTRACT

The search for successful therapies of infections with the coronavirus SARS-CoV-2 is ongoing. We tested inhibition of host cell nucleotide synthesis as a promising strategy to decrease the replication of SARS-CoV-2-RNA, thus diminishing the formation of virus progeny. Methotrexate (MTX) is an established drug for cancer therapy and to induce immunosuppression. The drug inhibits dihydrofolate reductase and other enzymes required for the synthesis of nucleotides. Strikingly, the replication of SARS-CoV-2 was inhibited by MTX in therapeutic concentrations around 1 μM, leading to more than 1000-fold reductions in virus progeny in Vero C1008 (Vero E6) and ~100-fold reductions in Calu-3 cells. Virus replication was more sensitive to equivalent concentrations of MTX than of the established antiviral agent remdesivir. MTX strongly diminished the synthesis of viral structural proteins and the amount of released virus RNA. Virus replication and protein synthesis were rescued by folinic acid (leucovorin) and also by inosine, indicating that purine depletion is the principal mechanism that allows MTX to reduce virus RNA synthesis. The combination of MTX with remdesivir led to synergistic impairment of virus replication, even at 100 nM MTX. The use of MTX in treating SARS-CoV-2 infections still awaits further evaluation regarding toxicity and efficacy in infected organisms, rather than cultured cells. Within the frame of these caveats, however, our results raise the perspective of a two-fold benefit from repurposing MTX for treating COVID-19. Firstly, its previously known ability to reduce aberrant inflammatory responses might dampen respiratory distress. In addition, its direct antiviral activity described here would limit the dissemination of the virus.

1. Introduction

The SARS-CoV-2 pandemic has so far infected > 160 million people, with > 3.4 million deaths ascribed to COVID-19 so far (May 2021). The fast spread of the virus raises the need for readily available therapies, preferably through drug repurposing. In addition to viral proteins, cellular pathways represent attractive targets, with fewer opportunities for viruses to develop drug resistance.

The life cycle of SARS-CoV-2 comprises the replication of the viral RNA genome, one of the longest single strand RNA genomes among all viruses. Large amounts of RNA need to be synthesized, often subgenomic for translation at ribosomes, as well as full-length RNA genomes for

* .
E-mail address: mdobbel@uni-goettingen.de (M. Dobbelstein).
[1] Equally contributing first authors.

https://doi.org/10.1016/j.virusres.2021.198469
Received 8 March 2021; Received in revised form 27 May 2021; Accepted 28 May 2021
Available online 6 June 2021

incorporation into virus progeny. Thus, high amounts of ribonucleotides are required in infected cells for virus replication. This makes nucleotide biosynthesis an attractive target for drugs to interfere with the propagation of the virus in infected individuals.

One way of suppressing nucleotide biosynthesis consists in the use of folate antagonists. This class of drugs, upon cellular uptake, diminishes the regeneration of tetrahydrofolate (THF) from dihydrofolate (DHF), and the subsequent transfer of methyl groups required for the synthesis of purine nucleotides, as well as desoxythymidine monophosphate and S-adenosyl methionine. Especially the lack of purine nucleotides can be expected to diminish the synthesis of virus RNA. Folate antagonists have not been broadly evaluated as antivirals, with the exception of some flaviviruses (Beck et al., 2019; Fischer et al., 2013). In contrast, sulfonamides and trimethoprim are routinely used for treating bacterial infections, and their mechanism of action is to prevent the synthesis of folic acid in bacteria (Estrada et al., 2016).

Methotrexate (MTX), along with the closely related aminopterin, represents the most established antifolate to act on eukaryotic cells. They belong to the earliest cancer drugs whatsoever, since they were first characterized by Sidney Farber and colleagues in the forties of the last century (Farber et al., 1948), and have been in clinical use ever since. They were first applied at high doses to treat leukemia as well as solid malignancies. Later, however, they were found to suppress the inflammatory and immune response even at low doses (Cronstein and Aune, 2020). Until today, MTX is broadly used to treat rheumatoid arthritis and other autoimmune diseases, and it is also part of current standard anti-cancer regimens. It is bioavailable orally and parenterally, inexpensive, and, with seven decades of clinical use, one of the best-characterized drugs in the clinics. Its disadvantages are often a result of long-term treatment, which would not be necessary in the case of treating an acute virus infection. Of note, however, pregnancy is a contraindication for MTX, due to its negative impact on fast-proliferating embryonal cells (Weber-Schoendorfer et al., 2014). Moreover, high doses of MTX can cause severe mucositis (den Hoed et al., 2015). Thus, therapies with MTX do require close monitoring by trained personnel.

Here we show that MTX reduces SARS-CoV-2 replication up to 1000-fold, at concentrations that are clinically achievable, in Vero cells as well as Calu-3 cells that resemble bronchial epithelial cells. This effect of MTX can be largely ascribed to impaired purine synthesis. Furthermore, MTX synergizes with the antiviral purine analogue remdesivir to diminish virus replication. Thus, MTX might not only reduce inflammation in the context of COVID-19 but also display a direct antiviral activity.

2. Materials & methods

2.1. Cell culture

Vero E6 cells (Vero C1008) were kindly provided by C. Stahl-Hennig, German Primate Center Göttingen, Germany. Cells were maintained in Dulbecco's modified Eagle's medium (DMEM with GlutaMAX™, Gibco) supplemented with 10% fetal bovine serum (Merck), 50 units/ml penicillin, 50 μg/ml streptomycin (Gibco), 2 μg/ml tetracycline (Sigma) and 10 μg/ml ciprofloxacin (Bayer) at 37 °C in a humidified atmosphere with 5% CO_2. The human lung epithelial cell line Calu-3 was purchased from ATCC (HTB-55) and maintained in Eagle's Minimum Essential Medium (EMEM, ATCC) supplemented with 10% fetal bovine serum and penicillin/streptomycin. Cells were routinely tested and ensured to be negative for mycoplasma contamination.

2.2. Virus stock production

SARS-CoV-2 was isolated from a patient sample taken in March 2020 at Göttingen, Germany. Throat swab material was mixed with medium containing 2% fetal bovine serum and used to inoculate Vero E6 cells for five days. The supernatant was passaged twice more to expand the virus. This cell culture supernatant was titrated for virus quantification by immunofluorescence analysis to contain 300,000 fluorescent focus units (FFU)/mL according to established protocols (Payne et al., 2006; Amarilla et al., 2021) and by qRT-PCR (Fig. 1B), and this was used as our virus stock in all experiments.

2.3. Treatments and SARS-CoV-2 infection

30,000 cells per well were seeded into 24-well-plates using medium containing 2% fetal bovine serum and incubated for 8 h at 37 °C. Cells were treated with methotrexate (Selleckchem S1210), remdesivir (Selleckchem S8932), palbociclib (Sigma-Aldrich PZ0199), leucovorin (Selleckchem S1236) and inosine (Selleckchem S2442) at the concentrations indicated in the figure legends. When preparing stock solutions, methotrexate and remdesivir were dissolved in DMSO; palbociclib, leucovorin and inosine in water. After 24 h, the cells were infected with virus stocks corresponding to 1×10^7 RNA-copies of SARS-CoV-2 (= 30 FFU, corresponding to the high particle-to-PFU ratio observed for SARS-CoV-2 previously (McCormick and Mermel, 2021)) and incubated for 48 h at 37 °C.

To determine the Median Tissue Culture Infectious Dose ($TCID_{50}$) per mL, 30,000 Vero E6 cells per well were pre-treated with MTX for 24 h, infected with 30,000 PFU for 1 hour and again treated with MTX for further 48 h. The virus-containing supernatant was titrated (end point dilution assay) to calculate the $TCID_{50}$/mL.

The IC50 value was calculated using the AAT Bioquest tool (www.aatbio.com/tools/ic50-calculator) and data from Fig. 2E.

2.4. Quantitative RT-PCR for virus quantification

For RNA isolation, the SARS-CoV-2 containing cell culture supernatant was mixed (1:1 ratio) with the Lysis Binding Buffer from the Magnapure LC Kit # 03038505001 (Roche) containing > 3 M guanidine thiocyanate (GTC), and the viral RNA was isolated using Trizol LS. After adding chloroform, the RNA-containing aqueous phase was isolated, and RNA was precipitated using isopropanol. The RNA pellet was washed with ethanol, dried and resuspended in nuclease-free water. Quantitative RT-PCR was performed according to a previously established RT-PCR assay involving a TaqMan probe (Corman et al., 2020), to quantify virus yield. The following oligonucleotides were purchased from Eurofins:

Oligonucleotide/ Gene	Sequence	Modification
P/E	ACA CTA GCC ATC CTT ACT GCG CTT CG	5′FAM, 3′BBQ
F/E	ACA GGT ACG TTA ATA GTT AAT AGC GT	
R/E	ATA TTG CAG CAG TAC GCA CAC A	
P/RdRP	CAGGTGGAACCTCATCAGGAGATGC	5′FAM, 3′BBQ
F/RdRP	GTGAAATGGTCATGTGTGGCGG	
R/RdRP	CAAATGTTAAAAACACTATTAGCATA	

Primers that amplify a genomic region corresponding to the envelope protein gene (26,141-26,253) were used for all experiments unless indicated otherwise. Primers that detect the RdRP/NSP12 coding region (15,361-15,460) were used to confirm the results obtained with the first primer set, as shown in Supplementary Figure 1.

The amount of SARS-CoV-2 RNA found upon infection without any drug treatment was defined as 100%, and the other RNA quantities were normalized accordingly.

2.5. Immunofluorescence analyses

Vero E6 cells were seeded onto 8-well chamber slides (Nunc) or 96-well plates (Corning) and treated/infected as indicated. After 48 h, the cells were fixed with 4% formaldehyde in PBS for 1 hour at room

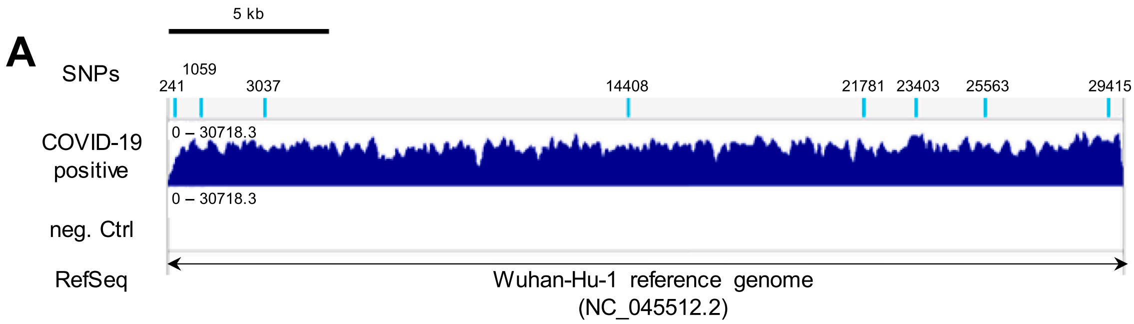

Sequencing and alignment statistics

Condition	Technical replicate	Total number of reads	Overall alignment rate [%]	Average read coverage per base (merged replicates)
neg. Ctrl	replicate 1	50,364,252	0.04	178 reads
	replicate 2	52,073,268	0.04	
COVID-19 positive	replicate 1	39,359,563	97.04	7903 reads
	replicate 2	40,751,048	97.17	

Mutational analysis of GOE_001

Reference	Position [base]	Nucleotide Wuhan-Hu-1	Nucleotide GOE_001	Amino acid substitution
NC_045512.2	241	C	U	5' UTR
	1059	C	U	T265I in Nsp2
	3037	C	U	Silent mutation (F)
	14,408	C	U	P323L in RdRp
	21,781	C	U	Silent mutation (T)
	23,403	A	G	D614G in Spike protein
	25,563	G	U	Q57H in ORF3a
	29,415	C	U	Silent mutation (S)

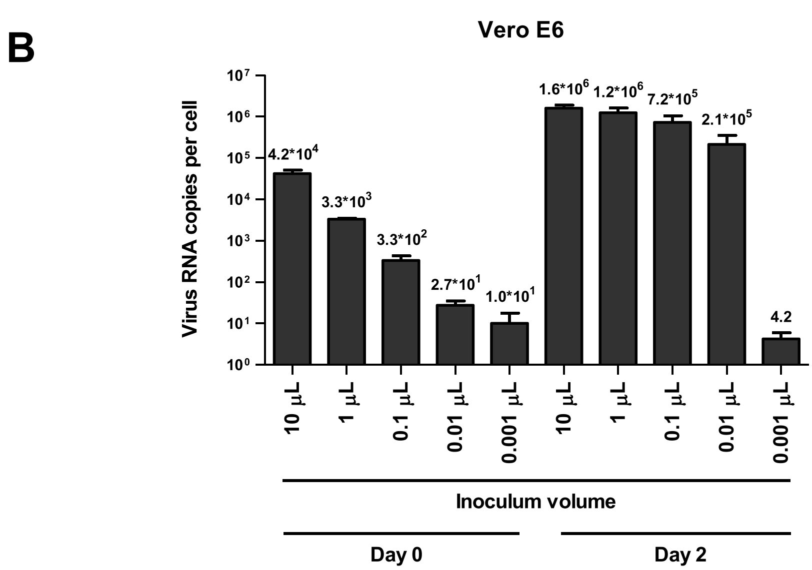

Fig. 1.. Characterization of a SARS-CoV-2 isolate (A)
Visualization of sequencing reads obtained from cell culture supernatants after infection with a sample of a COVID-19 positive patient (March 2020, Göttingen, Germany) and a non-infected cell monolayer (neg. Ctrl), mapped against the Wuhan-Hu-1 reference genome (NC_045512.2). Single nucleotide polymorphisms (SNPs) identified in the isolated SARS-CoV-2 strain (GOE_001) are indicated at the respective genomic positions as light blue bars on top of the read coverage. The tables underneath the genomic tracks describe the general sequencing and alignment statistics as well as the genetic alterations found. (B)
Viral RNA copies found in the supernatant after inoculating 30,000 Vero cells with the indicated amounts of the primary virus stock (300,000 Fluorescent Focus Units (FFU)/mL). The amounts of RNA per infected cell were determined by RT-PCR in the day 0 inoculum and compared to the virus-derived RNA in the cell culture supernatant after two days of infection. Note that more than 10^6 RNA copies were synthesized and released to the media per infected cell.

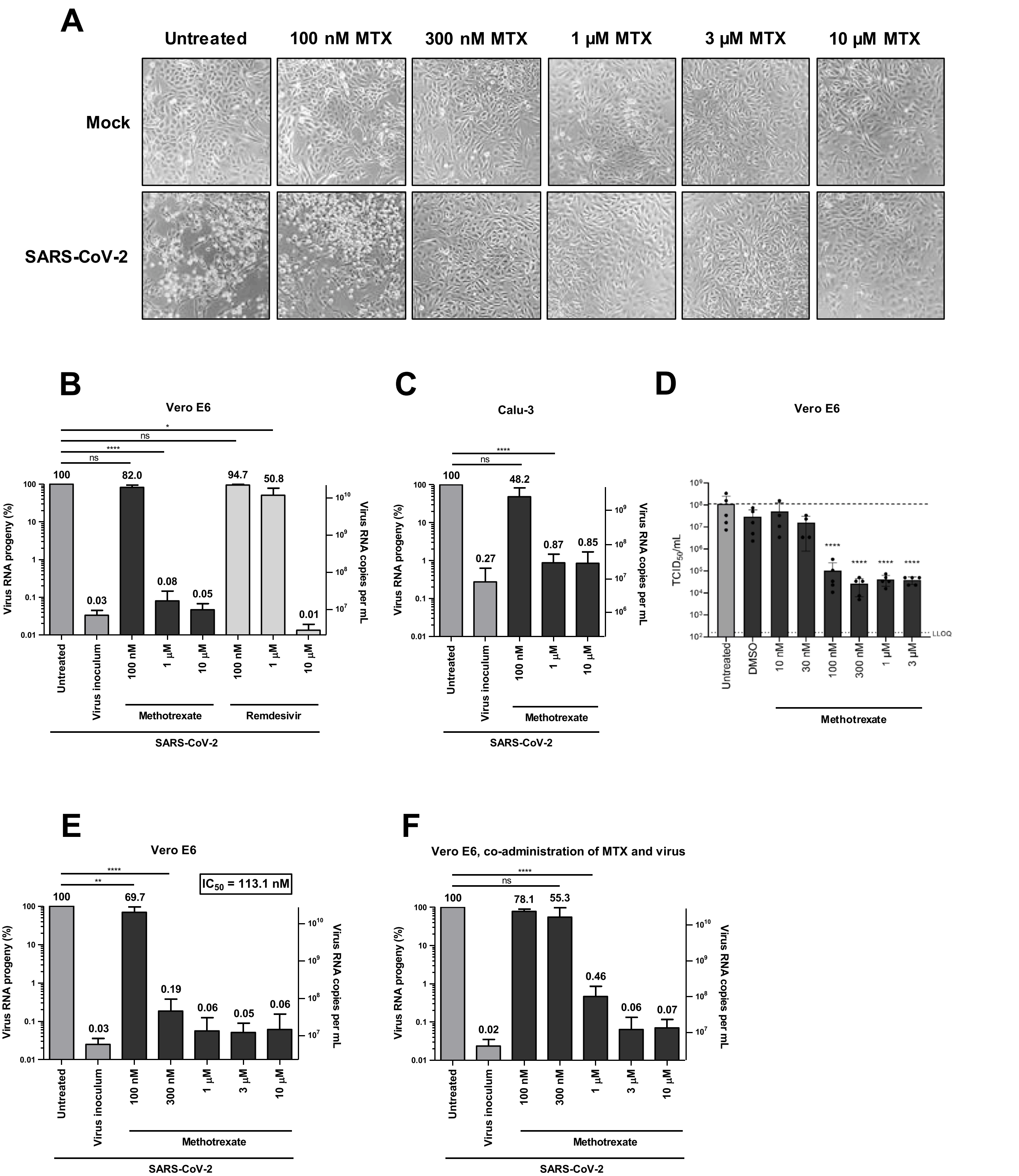

(caption on next page)

Fig. 2.. Impact of MTX on SARS-CoV-2 replication (A)
Diminished cytopathic effect (CPE) by MTX. 30.000 Vero cells were seeded, treated with MTX or the DMSO control, inoculated with the virus stock equivalent to 1 × 10^7 copies of RNA or 30 FFU/ MOI 0.001 and further incubated for 48 hrs. Cell morphology was assessed by phase contrast microscopy. Where indicated, the cells were treated with MTX at the indicated concentration for 24 hrs before and then throughout the time of infection. Note that the CPE was readily visible when comparing mock-infected and virus-infected cells, but only to a far lesser extent when the cells had been incubated with MTX. (B)
Diminished virus progeny by MTX. Vero cells were treated with MTX/remdesivir and/or infected as above. At 48 hrs post infection (p.i.), RNA was prepared from the cell supernatant, followed by quantitative RT-PCR to detect virus RNA. The amount of RNA found upon infection without MTX treatment was defined as 100%, and the other RNA quantities were normalized accordingly. MTX was found capable of reducing virus RNA yield by more than 1000-fold. Moreover, virus replication was more sensitive to equivalent concentrations of MTX than of remdesivir (mean with SD, $n = 3$). (C)
Reduced virus yield by MTX in Calu-3 cells. Calu-3 cells were treated with MTX and/or infected as above. Again, MTX reduced the amount of virus RNA released to the supernatant by more than 100-fold (mean with SD, $n = 3$). (D)
Reduced Median Tissue Culture Infectious Dose ($TCID_{50}$) by MTX. Vero cells were treated with MTX for 24 hrs before and then throughout the time of infection. Cells were infected with 30,000 PFU per well and further incubated for 48 hrs. The supernatant was titrated to determine the $TCID_{50}$/mL. LLOQ, Lower Limit of Quantification. (E and F)
MTX diminished virus progeny even when added to cells simultaneously with the virus. Vero cells were pre-treated with MTX and/or infected as above (E, mean with SD, $n = 8$) or only treated at the same time as they were infected (F, mean with SD, $n = 3$). The IC_{50} value was calculated using data from Fig. 2E.

temperature, permeabilized with 0.5% Triton X-100 in PBS for 30 min and blocked in 10% FBS/PBS for 10 min. Primary antibodies were used to stain the SARS-CoV-2 Spike (S; GeneTex #GTX 632604, 1:2000) and Nucleoprotein (N; Sino Biological #40143-R019, 1:5000) overnight. Secondary Alexa Fluor 488 donkey anti-mouse IgG and Alexa Fluor 546 donkey anti-rabbit IgG (Invitrogen, 1:500) antibodies were added together with 4′,6-diamidino-2-phenylindole (DAPI) for 1.5 h at room temperature. All antibodies were diluted in blocking solution. Slides with cells were mounted with Fluorescence Mounting Medium (DAKO) and fluorescence signals were detected by microscopy (Zeiss Axio Scope. A1). Automated high-content immunofluorescence microscopy was performed with the BD Pathway™ 855 (Becton Dickinson) using the AttoVision image acquisition software (Becton Dickinson) to quantify the amount of SARS-CoV-2 positive cells. In this single-cell-based image analysis, the DAPI signal was used to identify and count cell nuclei, whereas the Alexa Fluor 546 (N protein) intensity per cell was quantified within a ring around the nuclei.

2.6. ATP quantification by luminometry

10,000 Vero E6 cells per well were seeded into 24-well plates, treated with DMSO or MTX and infected with SARS-CoV-2 as indicated. After 48 h, the cells were lysed with the Lysis Binding Buffer from the Magnapure LC Kit 03038505001 (Roche) containing > 3 M guanidine thiocyanate (GTC), and ATP levels were quantified by adding luciferase as well as luciferin to a 1 µl sample of the lysate, using 100 µl of the CellTiter-Glo® Luminescent Cell Viability Assay solution (Promega), followed by luminometry using a Centro LB 960 luminometer (Berthold).

2.7. Immunoblot analysis

Cells were washed once in PBS and harvested in radio-immunoprecipitation assay (RIPA) lysis buffer (20 mM TRIS-HCl pH 7.5, 150 mM NaCl, 10 mM EDTA, 1% Triton-X 100, 1% deoxycholate salt, 0.1% SDS, 2 M urea) in the presence of protease inhibitors. Samples were briefly sonicated to disrupt DNA-protein complexes. The protein extracts were quantified using the Pierce BCA Protein assay kit (Thermo Fisher Scientific). Protein samples were boiled at 95 °C in Laemmli buffer for 5 min, and equal amounts were analyzed by sodium dodecyl sulfate polyacrylamide gel electrophoresis (SDS-PAGE). Subsequently, proteins were transferred onto a nitrocellulose membrane, blocked in 5% (w/v) non-fat milk in TBS containing 0.1% Tween-20 for 1 hour and incubated with primary antibodies at 4 °C overnight followed by incubation with peroxidase-conjugated secondary antibodies (donkey anti-rabbit or donkey anti-mouse IgG, Jackson Immunoresearch). The proteins were detected using either Super Signal West Femto Maximum Sensitivity Substrate (Thermo Fisher) or Immobilon Western Substrate (Millipore).

Antibody	Source (Catalogue number)	Concentration
SARS-CoV-2 Spike	GeneTex GTX 632604	1:1000
SARS-CoV-2 Nucleoprotein	Sino Biological 40143-R019	1:5000
DHFR	Abcam ab124814	1:10,000
Actin	Abcam ab6276	1:40,000
GAPDH	Abcam ab8245	1:5000
Hsc70	Santa Cruz sc-7298	1:15,000
p53	Santa Cruz sc-126	1:500
p21	Cell Signaling cs#2947	1:1000
CDK4	Abcam ab68266	1:500

2.8. Cell counts (Celigo)

Vero E6 cells were seeded into 24-well-plates and treated/infected as indicated. After fixation of the cells and DAPI staining to visualize nuclear DNA, the numbers of nuclei were counted automatically using the Celígo® S Imaging Cytometer (Nexcelom Bioscience).

2.9. Quantification of LDH release to determine cytotoxicity

3500 Vero E6 cells were seeded onto 96-well-plates and treated with MTX and/or remdesivir as indicated for 72 h. Lactate dehydrogenase (LDH) is a cytosolic enzyme that is released into the cell culture supernatant upon disruption of the plasma membrane and was used to determine cytotoxicity. The LDH release into the cell culture medium was measured and quantified by bioluminescence using the LDH-Glo™ Cytotoxicity Assay kit (Promega). 2 µL of 10% Triton X-100 were added to untreated cells for 10 min to determine the maximum LDH release. Percent cytotoxicity reflects the proportion of LDH released to the media (compared to the overall amount of LDH in the cells) and was calculated using the following formula:

$$\text{Cytotoxicity}(\%) = 100 \times \frac{(\text{Experimental LDH Release} - \text{Medium Background})}{(\text{Maximum LDH Release Control} - \text{Medium Background})}$$

2.10. Flow cytometry

For cell cycle analysis, cells were harvested in cold storage buffer (1% FBS in PBS) after treatment/infection, fixed in ethanol, and stained with propidium iodide (Sigma-Aldrich). Cell cycle profiles were generated using a Guava EasyCyte Plus system (Millipore) and analyzed by using the Cyto Soft 5.3 software.

2.11. RNA sequencing and NGS data analysis

Quality and integrity of RNA were assessed using the Fragment

Analyzer (Advanced Analytical) and the standard sensitivity RNA Analysis Kit (DNF-471). RNA-seq libraries were prepared using a non-stranded RNA Seq, massively-parallel mRNA sequencing approach (Illumina; TruSeq RNA Library Preparation Kit v2, Set A; 48 samples, 12 indexes, Cat. N°RS-122–2001). Specifically, we first optimized the ligation step diluting the concentration of adaptors to increase ligation efficiency (>94%), and we reduced the number of PCR cycles (10 cycles) to avoid PCR duplication artifacts as well as primer dimers in the final library product. Libraries were prepared on an automated device (Beckman Coulter's Biomek FXP workstation). For accurate quantitation of cDNA libraries, a fluorometry-based system, the QuantiFluor™dsDNA System (Promega) was used. The size of final cDNA libraries was determined using the dsDNA 905 Reagent Kit (Fragment Analyzer from Advanced Bioanalytical) revealing sizes of 280 bp on average. Libraries were pooled and sequenced on the Illumina HiSeq 4000 analyzer (PE; 1 × 2 × 150 bp; 80 Mio reads/sample). Sequence images were transformed using the software BaseCaller (Illumina) to obtain BCL files, which were demultiplexed to FASTQ files using bcl2fastq v2.20.

Analysis of sequencing data was performed on the high-performance computing cluster provided by the Gesellschaft für wissenschaftliche Datenverarbeitung mbH Göttingen (GWDG) using the software Xshell® 6 for Home/School (NetSarang Computer Inc.). FASTQ files were subjected to quality control using FASTQC/0.11.4 (Babraham Bioinformatics) prior to trimming using FASTX/0.0.14 (Hannon Lab) according to following thresholds: first base to keep: 15, last base to keep: 140. Trimmed read pairs were mapped against the SARS-CoV-2 Wuhan-Hu-1 reference genome (accession number: NC_045512.2) (Wu et al., 2020) using BOWTIE2/2.3.4.1 (Langmead and Salzberg, 2012) with the –very-sensitive end-to-end setting. Resulting SAM files were processed using SAMTOOLS/1.9 (Li, 2011). In short, SAM files were converted into BAM files using samtools view, followed by merging of technical replicates using samtools merge. The resulting BAM files were subsequently re-sorted according to genomic coordinates using samtools sort, PCR duplicates were removed using samtools markdup with default settings, and the corresponding index files were generated using samtools index. Sequencing depth was determined using samtools depth and the average read coverage per base was calculated taking the average sequencing depth for all positions across the reference genome. Genomic tracks of mapped reads were calculated using the bamCoverage function of DEEPTOOLS/3.0.1 (Ramirez et al., 2016) with the following settings: -e 100, –ignoreDuplicate, –smoothLength 60, –binSize 20, –samFlagInclude 64. SNPs present in the isolated virus were identified using bcftools mpileup with default settings, followed by bcftools call with -mv and -Ob settings of BCFTOOLS/1.9 (Samtools). Identified variants were filtered and converted into VCF files using bcftools view with the -i '%QUAL>=150′ setting. Genomic tracks as well as VCF files were visualized using the Integrative Genomics Viewer v2.3 (Robinson et al., 2017; Robinson et al., 2011; Thorvaldsdóttir et al., 2013).

2.12. Quantification and statistical analysis

Statistical testing was performed using Graph Pad Prism 6 (RRID: SCR_002798). A two-sided unpaired Student's *t*-test was calculated. Significance was assumed where p-values ≤ 0.05. Asterisks represent significance in the following way: ****, $p \leq 0.0001$, ***, $p \leq 0.005$; **, $p \leq 0.01$; *, $p \leq 0.05$.

3. Results

3.1. Infection with SARS-CoV-2 produces $>10^6$ copies of genomic virus RNA per cell

We isolated SARS-CoV-2 from a patient sample taken in March 2020 at Göttingen, Germany. Throat swab material was used to inoculate Vero C1008 cells (i.e. Vero E6 cells; shortly termed Vero cells from here on). The supernatant was passaged twice more to expand the virus, and cell supernatant was subjected to deep sequencing analysis. More than 80×10^6 reads, 2×150 bp each, were taken and aligned with the published genome sequence of the first Wuhan strain of SARS-CoV-2 (Wu et al., 2020). >97% of all reads corresponded to the virus. Comparing the Göttingen and Wuhan strains, only 8 nucleotide deviations were found (Fig. 1A). Most of these deviations were from C to U, arguing that they might have occurred through RNA deamination rather than misincorporation by the polymerase. Among the deviations was a nucleotide exchange leading to the mutation D614G in the Spike (S) protein that was recently reported to increase the number of S proteins displayed on the viral envelope (Zhang et al., 2020; Li et al., 2021). Of note, however, no change in the coding region for the furin cleavage site of the S protein (Hoffmann et al., 2020; Ogando et al., 2020; Liu et al., 2020) was observed.

Next, we detected and quantified the viral RNA released from infected cells. With decreasing virus inoculate, the yield of virus progeny after two days first remained at a maximum and then steeply decreased (Fig. 1B). The decrease in virus yield was more than linear compared to the decrease in inoculum. This may be explained by a high proportion of virus particles that do not successfully undergo a full infectious cycle, as noticed earlier (McCormick and Mermel, 2021). Alternatively or in addition more than one virus particle might be required for the productive infection of a cell, leading to a more than proportional decrease in infectivity with lower virus concentrations. Quantitative RT-PCR of a genomic fragment comprising the Envelope protein coding region (Corman et al., 2020) with comparison to a standard (kind gift by M. L. Schmidt, Robert Koch Institute, Berlin, Germany) revealed that up to 1.6×10^6 copies of viral genomic RNA were released from each cell in the infected culture. This was confirmed (Suppl. Fig. 1) by using an additional primer set that binds to a different portion of the virus genome to amplify a fragment close to the 5′ region of the positive genomic RNA (the RdRP/NSP12 coding region), which according to (Alexandersen et al., 2020) is hardly involved in subgenomic fragments. Given the length of the viral genome of roughly 3×10^4 nucleotides, this suggests that one infected cell needs to produce at least $3 \times 1.6 \times 10^{10} = 4.8 \times 10^{10}$ nucleotides for virus RNA synthesis – and this does not include subgenomic virus RNA to encode virus proteins, nor negative strand RNA intermediates. Hence, virus production requires at least 8 times more nucleotides than the replication of the cellular genome (6×10^9 nucleotides in a diploid human cell). By this calculation, the demand of virus replication on nucleotide biosynthesis corresponds to more than what is needed for the re-synthesis of all ribosomal RNAs, assuming 5×10^6 ribosomes per cell (Lewin, 1994; Milo et al., 2010) and 7×10^3 ribonucleotides per ribosome. Considering these numbers, we reasoned that nucleotide biosynthesis might represent a limiting factor for virus replication, and hence a suitable drug target.

3.2. MTX strongly diminishes virus yield upon infection with SARS-CoV-2

As a strategy to interfere with nucleotide biosynthesis, and hence with virus replication, we treated Vero cells with MTX 24 h before and during infection with SARS-CoV-2. Strikingly, the treatment with MTX strongly antagonized the infection. MTX largely prevented the cytopathic effect (CPE) observed in infected cells, whereas up to 10 μM MTX did not produce obvious morphologic signs of cytotoxicity (Fig. 2A), in agreement with recent reports (Xing et al., 2020; Caruso et al., 2020). The amount of virus RNA released into the media was reduced up to 1000-fold by MTX in Vero cells (Fig. 2B), and the effective concentration of MTX was around 1 μM, which was lower than the effective concentration of the established antiviral drug remdesivir, i.e. 10 μM (Fig. 2B). MTX diminished SARS-CoV-2 progeny up to 100-fold in Calu-3 cells (Fig. 2C), a cell line that can be used to model bronchial epithelia (Foster et al., 2000). Moreover, similar results were obtained when the TCID50 (Median Tissue Culture Infectious Dose)/ml was determined as a readout for virus yield (Fig. 2D). Most notably, MTX did not only reduce virus yield in Vero cells that were treated 24 h before virus infection (Fig. 2E), but also diminished virus progeny in cells that were only treated with MTX right at the time of SARS-CoV-2 infection (Fig. 2F) and even when MTX was added 4 h after infection (Suppl. Fig. 2). Taken together, these results indicate that MTX is a potent inhibitor of SARS-CoV-2 replication.

3.3. In the presence of MTX, far lower amounts of virus proteins accumulate in SARS-CoV-2-infected cells

To obtain a first idea about the stage of the infectious cycle affected by MTX, we detected viral proteins upon treating the cells with MTX and infecting them with SARS-CoV-2. The detection rate of viral nucleoprotein and thus the rate of SARS-CoV-2 positive cells was severely reduced by MTX as determined by immunofluorescence microscopy (Fig. 3A, B). In accordance with this observation, immunoblot analysis of Vero cells revealed that infected cells contained high amounts of the viral N and S proteins, whereas the amounts of these proteins were strongly diminished by MTX (Fig. 3C). This argues that not just the release of virus particles is diminished by MTX, but also the earlier steps of the infectious cycle, i.e. the synthesis of virus proteins.

3.4. The antiviral effect of MTX is a result of defective purine synthesis but not phenocopied by CDK inhibition

MTX can slow down cell cycle progression (Tsurusawa et al., 1990). Accordingly, cells treated with MTX proliferated more slowly compared to untreated control cells but did not increase the release of LDH, indicating that the cytotoxicity levels remain unchanged upon MTX treatment (Fig. 4A). To determine whether a cell cycle arrest might be accountable for decreased virus replication upon MTX treatment, we performed flow cytometry and compared MTX with palbociclib, a selective inhibitor of the cyclin-dependent kinases CDK4 and CDK6 (Klein et al., 2018). Compared to the control, MTX treatment increased the levels of the tumor suppressor p53 and its target gene product p21, as

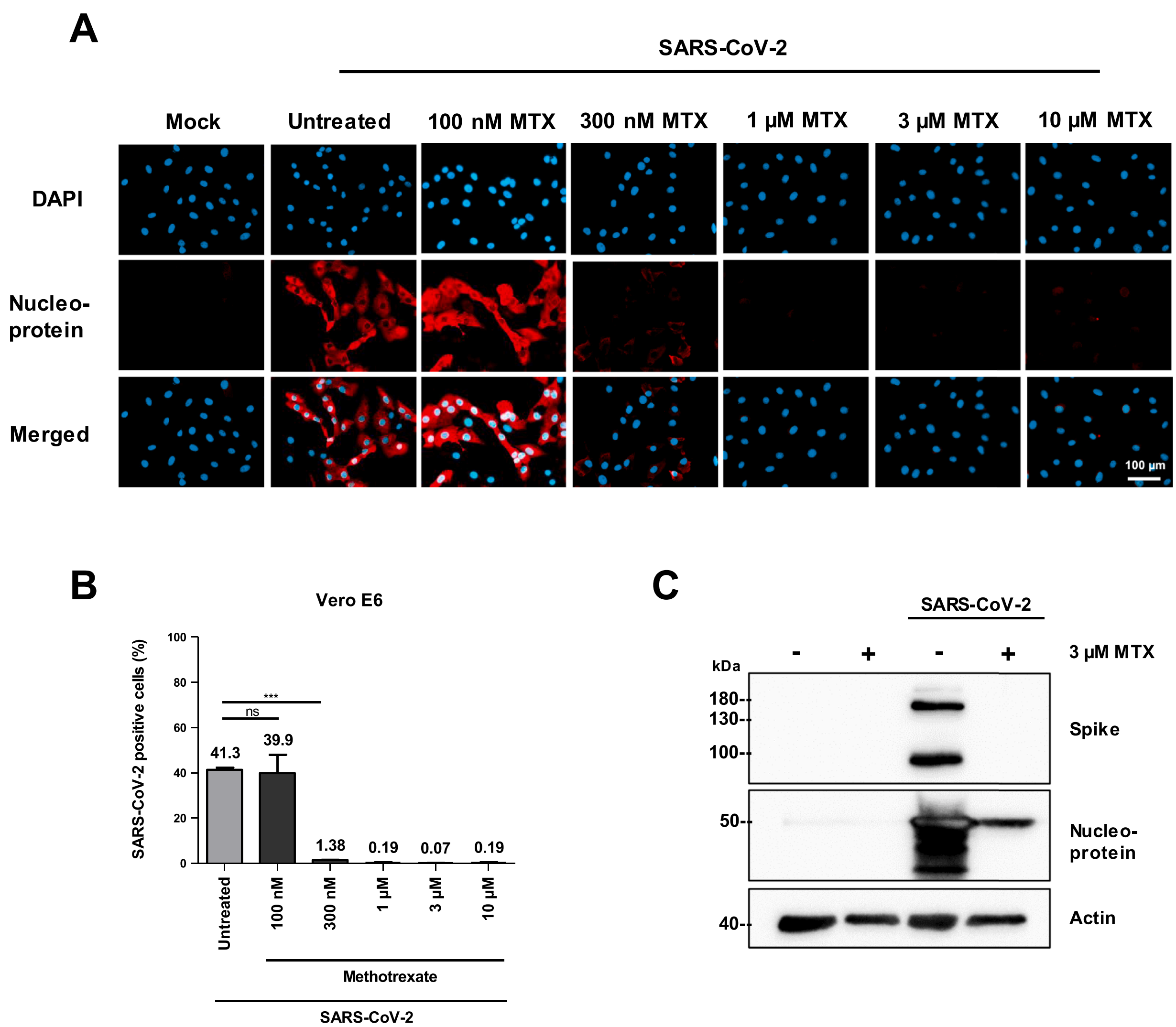

Fig. 3.. Reduction of viral protein synthesis by MTX (A)
Representative images showing the reduction of viral protein synthesis by MTX. Vero cells were treated with MTX as indicated and infected with SARS-CoV-2 as in Fig. 2. Cell nuclei were stained with DAPI, and the SARS-CoV-2 Nucleoprotein was detected by immunofluorescence. (B)
Reduction of the infected cell fraction by MTX. Vero cells were treated and/or infected as in Fig. 2. The cell nuclei and the SARS-CoV-2 Nucleoprotein were detected and quantified by high-content fluorescence microscopy. For each cell, a mask was created automatically to measure the intensity of the nucleoprotein staining and thereby determine the proportion of SARS-CoV-2-positive cells. Average and standard deviation of two replicates, each performed in eight technical replicates, are depicted. (C)
Decreased virus protein synthesis in the presence of MTX. Upon MTX treatment and/or infection of Vero cells as in Fig. 2, the viral S and N proteins as well as actin (loading control) were detected by immunoblot analysis.

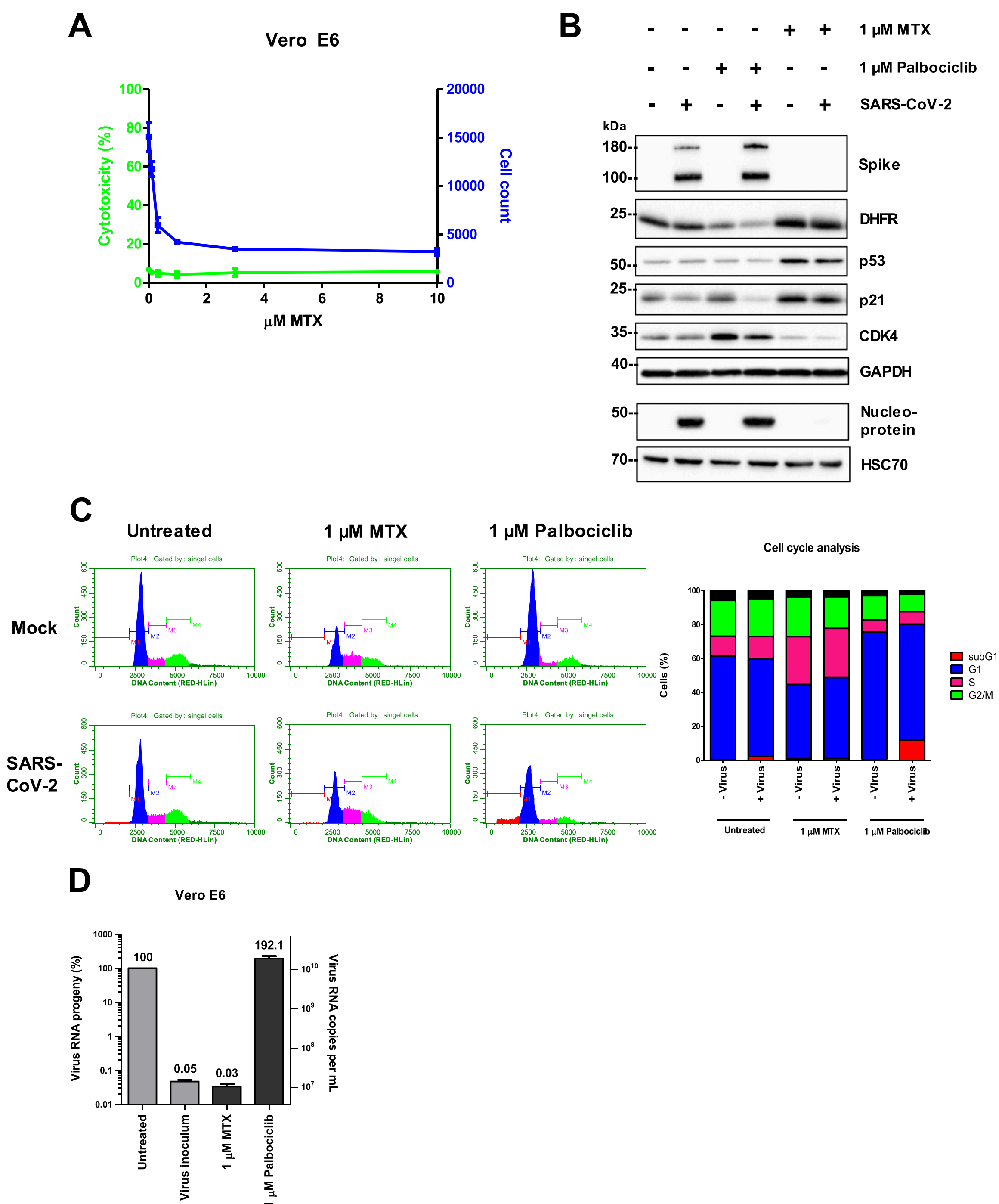

Fig. 4.. Excluding cell cycle arrest as the major antiviral mechanism of MTX (A)
Lack of measurable cytotoxicity by MTX. Vero cells were treated with MTX at the indicated concentration for 72 hrs. The release of lactate dehydrogenase (LDH) to the supernatant was quantified by bioluminescence as a read-out for cytotoxicity. The percentages reflect the proportion of LDH released to the media, compared to the overall amount of LDH in the cells. The number of cells per well were quantified by the Celígo® S Imaging cytometer. Note that the number of cells was reduced after treatment with higher concentrations of MTX but cytotoxicity levels remained unchanged (mean with SD, $n = 3$). Thus, the CC50 (concentration to kill 50% of all cells) was never reached in these experiments, even with the highest concentration of MTX, i.e. 10 μM. The reported CC50 for MTX is >90 μM (Beck et al., 2019; Fischer et al., 2013). (B)
Increased levels of dihydrofolate reductase (DHFR), p53 and p21 upon MTX treatment, regardless of virus infection, accompanied by decreased virus protein synthesis in the presence of MTX. Upon MTX or palbociclib treatment and/or infection of Vero cells as in Fig. 2, the viral N and S proteins as well as DHFR, p53, p21, CDK4 and GAPDH (loading control) were detected by immunoblot analysis. Note that the virus protein levels remained unchanged upon palbociclib treatment. (C) Induction of a cell cycle arrest upon MTX and palbociclib treatment. Vero cells were treated with 1 μM MTX or palbociclib and infected with SARS-CoV-2 as in Fig. 2. Flow cytometry was performed to analyze cell cycle progression. Note that both drugs induced a cell cycle arrest and therefore impaired cell proliferation. (D) Reduction of virus RNA progeny by MTX but not palbociclib. Vero cells were treated with 1 μM MTX/palbociclib, infected as in Fig. 2. and the virus RNA was detected by quantitative RT-PCR. MTX was found capable of reducing virus RNA yield by more than 1000-fold, whereas palbociclib did not diminish virus replication (mean with SD, $n = 3$).

well as its target gene product dihydrofolate reductase (DHFR), as described (Hsieh et al., 2009). Palbociclib increased the levels of its target CDK4, as reported previously (Paternot et al., 2014) (Fig. 4B). Although both drugs impaired cell proliferation (Fig. 4C), palbociclib did not affect the synthesis of SARS-CoV-2 specific proteins (Fig. 4B) nor virus replication (Fig. 4D), indicating that the antiviral effect of MTX can not be explained solely by cell cycle arrest.

3.5. Folinic acid as well as purine nucleoside rescue virus replication in the presence of MTX

MTX interferes with a number of metabolic steps (Fig. 5A) after cellular uptake and polyglutamation (Cronstein and Aune, 2020; Alqarni and Zeidler, 2020; Bedoui et al., 2019). First and foremost, it inhibits dihydrofolate reductase (DHFR) (Nichol and Welch, 1950; Osborn et al., 1958). However, purine synthesis is inhibited by MTX even under conditions when the directly required folate metabolite, 10-formyl-THF, is largely preserved in its levels (Allegra et al., 1986). This argues that MTX diminishes purine synthesis, at least to a substantial extent, by direct inhibition of one of its metabolic steps. And indeed, polyglutamated MTX inhibits phosphoribosylaminoimidazolecarboxamide (AICAR) transformylase (ATIC) (CJ Allegra et al., 1985; Baggott et al., 1986). MTX, when polyglutamated, also inhibits thymidylate synthetase (TYMS) directly (CJ Allegra et al., 1985; Borsa and Whitmore, 1969), which, along with the depletion of 5, 10 methylene THF, further diminishes the synthesis of deoxythymidine monophosphate (Chu et al., 1990). This then reduces the availability of deoxythymidine triphosphate, which is required for the synthesis of DNA but not RNA. Finally, MTX also acts as an inhibitor of methylene tetrahydrofolate-reductase (MTHFR) (Chabner et al., 1985). In addition to the shortage of the MTHFR substrate 5,10 methylene THF, this direct inhibition reduces the regeneration of methionine from homocysteine. Methionine is required to synthesize S-adenosylmethionine (SAM), a necessary substrate of methylations of proteins (e.g. histones) as well as the RNA 5′-cap.

To determine the impact of MTX on the metabolism of infected cells, we asked whether purine synthesis might be diminished by MTX treatment in the context of infection. One key product of purine synthesis is represented by ATP. To determine ATP levels in MTX-treated and/or virus-infected cells, we rapidly lysed the cells in a chaotropic buffer, followed by dilution and addition of luciferin and luciferase to cell lysates, and luminometry. In this assay system, the levels of ATP are directly reflected by the extent of luminescence. Simultaneously, we determined the corresponding cell numbers by DAPI-staining of cell nuclei and automated quantification. When calculating the relative amount of ATP per cell, we found that MTX reduced ATP levels about three- to fivefold in infected as well as non-infected cells, suggesting that MTX impairs purine synthesis even upon infection with SARS-CoV-2 (Fig. 5B).

Next, we performed rescue experiments to elucidate the mechanism (s) required to interfere with virus replication.

First, we added folinic acid (leucovorin) to the cells along with the MTX treatment. Remarkably, this fully rescued virus replication. Folinic acid is readily converted to 5,10 methylene THF, thus re-supplying the source of methylation required by all MTX-inhibited reactions (Chan and Cronstein, 2010). The rescue strongly suggests that the impact of MTX on virus replication is indeed due to its competition with endogenous folic acid and its metabolism (Fig. 5C).

Moreover, the addition of inosine restored virus replication in the presence of MTX (Fig. 5D). Both leucovorin and inosine were also capable of re-establishing the synthesis of virus N and S proteins (Fig. 5E). Inosine is rapidly converted to inosine monophosphate (Chan and Cronstein, 2010; Kozminski et al., 2020), which otherwise represents the end point of purine synthesis. This indicates that purine synthesis, rather than the supply of thymidine or SAM, is critical for virus replication. From this, the reduced supply of ribonucleotides appears as the dominating mechanism of action allowing MTX to act in an antiviral fashion.

3.6. Remdesivir synergizes with MTX to antagonize SARS-CoV-2 replication

Remdesivir is currently one of the most advanced antiviral drugs against SARS-CoV-2 infection (Wang et al., 2020; Beigel et al., 2020), despite recent setbacks regarding its clinical impact (Spinner et al., 2020). It resembles a purine nucleoside and acts as an adenosine analogue to inhibit viral RNA polymerase. Since MTX diminishes the amounts of available ATP in SARS-CoV-2-infected cells (Fig. 5B), we reasoned that it might increase the incorporation of remdesivir and hence its antiviral activity. To test this, we first determined suboptimal concentrations of MTX and remdesivir to moderately diminish virus replication. Then, we treated Vero cells with the drugs at these concentrations, alone or in combination, followed by infection with SARS-CoV-2. And indeed, while each drug alone reduced the virus RNA in the cell supernatant (reflecting viral progeny) by roughly 50–75%, the combination of both drugs led to a reduction by more than 98% (Fig. 6A and Suppl. Fig. 3) without increasing cytotoxicity towards non-infected cells (Fig. 6B). Similarly, virus proteins were still detectable when the cells had been treated with single drugs at these concentrations, but the drug combination virtually extinguished the corresponding immunofluorescence signals (Fig. 6C). We conclude that MTX enhances the efficacy of remdesivir, leading to synergistic therapeutic efficacy.

4. Discussion

Our results indicate that MTX efficiently inhibits the propagation of SARS-CoV-2, at least in the cell culture systems under study here. The inhibitory effect of MTX primarily relies on reduced purine synthesis. Moreover, MTX was combined with remdesivir to yield synergistic virus inhibition. Pending further testing in animals, these results are compatible with the idea of repurposing MTX as a drug for treating and/or preventing COVID-19, combining its known anti-inflammatory with the here-described antiviral effect. However, MTX might be more effective in cells that allow SARS-CoV-2 to replicate in high levels, thus raising the need for lots of nucleotides. We anticipate that MTX might be less potent in cells where the virus only replicates in moderate copy numbers, e.g. in primary cells of bronchial epithelia.

While this paper was presented as a manuscript on biorxiv, independent work was published to indicate the ability of MTX to block SARS-CoV-2 replication as well (Caruso et al., 2020). On top of reporting this, our results provide additional insights into the impact of MTX on virus protein synthesis, the rescue by folic acid and purine, as well as the cooperative effect of MTX with remdesivir. Very recently, the interplay of SARS-CoV-2-infection and the metabolism of C1 bodies was elucidated in detail (Zhang et al., 2021) and this report also confirmed (and cited) the results provided in our study.

Of note, some virus replication was observed in the presence of even high amounts of MTX (as determined by qRT-PCR as well as TCID50, cf. Fig. 2). We propose that this is due to the use of existing purine nucleotides that are derived from degrading nucleic acids and the salvage pathway. This allows for a pool of nucleotides independent of purine synthesis, this pool may then be used for replicating a limited amount of virus RNA.

The principle of limiting nucleotide synthesis to interfere with virus replication might be further expanded to treat COVID-19. To limit the synthesis of guanine nucleotides, the enzyme inosine-5′-monophosphate dehydrogenase (IMPDH) can be inhibited by mycophenolic acid, an established drug in the clinics (Allison and Eugui, 1996), and this interferes with SARS-CoV-2 replication (Kato et al., 2020). Furthermore, pyrimidine synthesis can be reduced by inhibitors of orotate synthesis, targeting dihydroorotate dehydrogenase (DHODH). Besides teriflunomide, an approved immunomodulatory drug, novel DHODH

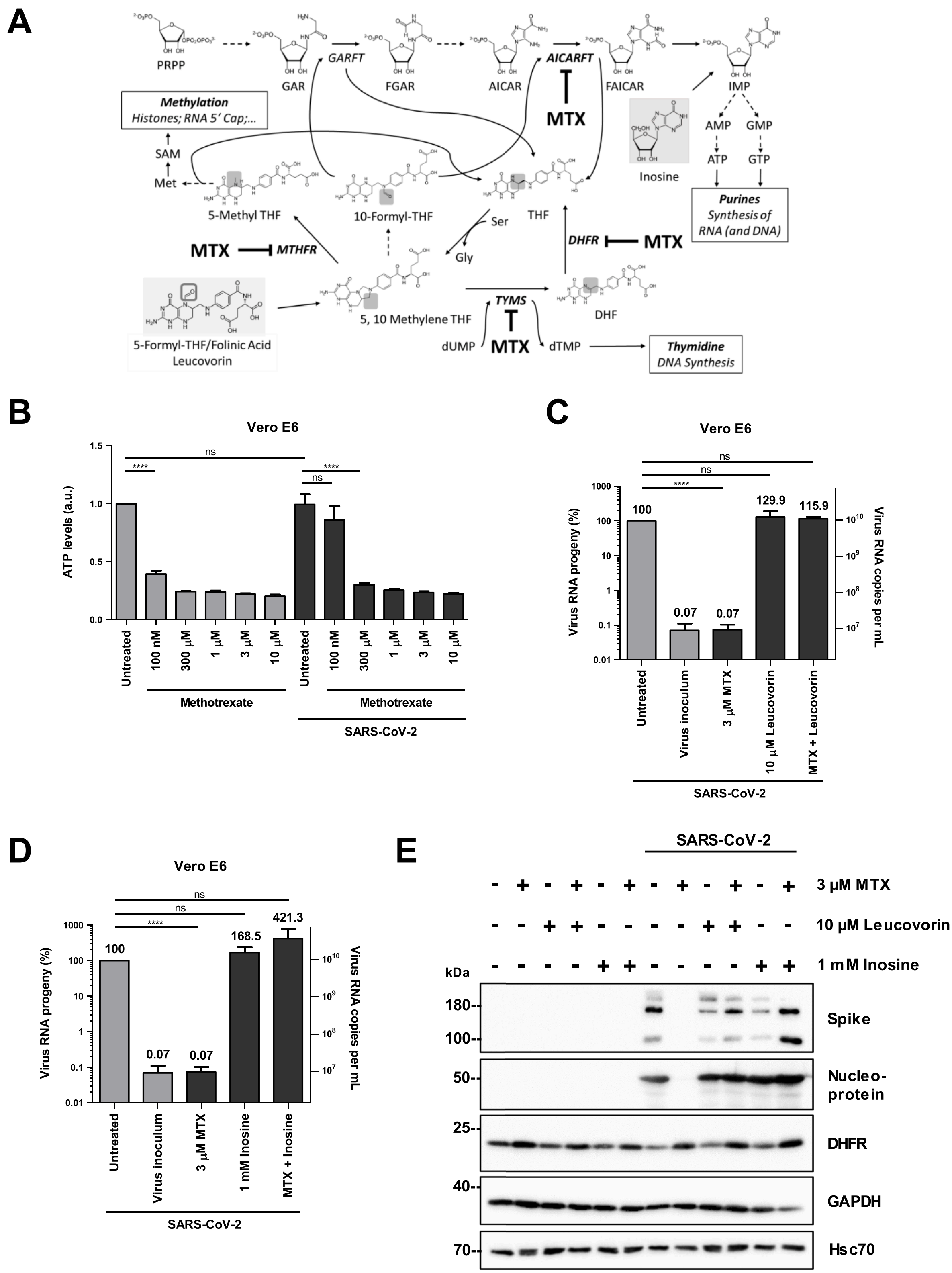

(caption on next page)

Fig. 5.. The antiviral effect of MTX is a result of defective purine synthesis, which can be rescued by folinic acid or a purine nucleoside (A)
Metabolic map indicating the major steps inhibited by MTX. *Enzymes* are indicated in *italics*. ***Enzymes directly inhibited by MTX*** are printed in ***bold and italics***. Plain arrows indicate direct reactions, dashed arrows indicate reactions with intermediates that are omitted for simplicity. Metabolites used for rescue experiments are shown with a gray background. Folic acid metabolites: DHF, dihydrofolate; THF, tetrahydrofolate. Folic acid metabolism, enzymes: *DHFR*, dihydrofolate reductases; *MTHFR*, methylene tetrahydrofolate reductase; *TYMS*, thymidylate synthetase. Purine synthesis, enzymes: *GARFT*, glycinamide ribonucleotide formyltransferase; *AICARFT*, 5-aminoimidazole-4-carboxamide ribonucleotide formyltransferase, part of the dual function enzyme ATIC (comprising AICARFT and IMP cyclohydrolase). Purine synthesis, metabolites: PRPP, phosphoribosyl pyrophosphate; GAR, glycinamide ribonucleotide; FGAR, formylglycinamide ribonucleotide; AICAR, 5-aminoimidazole-4-carboxamide ribonucleotide; FAICAR, 5-formamidoimidazole-4-carboxamide ribonucleotide. Nucleotides are indicated by standard abbreviations, i.e. IMP (inosine monophosphate), AMP, GMP, ATP, GTP, dUMP, dTMP. Amino acids are abbreviated as Ser, Gly, Met. (B)
ATP levels upon MTX-treatment and SARS-CoV-2 infection. Vero cells were treated with MTX as indicated and infected with SARS-CoV-2 as in Fig. 2. Cells were counted using the Celígo® S Imaging cytometer and ATP levels were measured by the CellTiter-Glo® assay. This experiment was performed on four separate plates with four technical replicates each (mean with SD). The extent of luminescence, reflecting relative ATP levels, was normalized to the number of cells found under the same conditions and further normalized to untreated and mock-infected cells. Thus, the columns reflect the relative amount of ATP per cell in each case. Note that SARS-CoV-2 infection as such did not significantly affect ATP levels. (C)
Rescue of virus replication in the presence of MTX by folinic acid (leucovorin). Vero cells were inoculated with virus as in Fig. 2, with or without MTX treatment 24 hrs before and during infection. In parallel or in addition, leucovorin was added to the cell culture media, at a concentration of 10 μM (mean with SD, $n = 3$). (D)
Restored virus replication by inosine, in the presence of MTX. The experiment was carried out as in (A), with the addition of 1 mM inosine instead of leucovorin (mean with SD, $n = 3$). (E)
Rescue of virus protein synthesis by leucovorin or inosine, in the presence of MTX. Upon treatment and infection of Vero cell as in (A) and (B), cell lysates were subjected to immunoblot analysis. The viral S and N proteins, DHFR as well as GAPDH and Hsc70 (loading controls) were detected.

inhibitors are in current clinical testing for treating cancer and leukemia (Madak et al., 2019). Recently, a DHODH inhibitor was also found active against SARS-CoV-2 (Luban et al., 2021; Coelho and Oliveira, 2020) and might be re-purposed for treating SARS-CoV-2 infections as well, e.g. through a recently completed phase I trial (NCT04425252).

In addition to purine synthesis, MTX also limits the transfer of C1 bodies (methyl groups) through MTHFR to regenerate S-adenosylmethionine (SAM), a major substrate for methyltransferases in the cell (Cronstein and Aune, 2020). Since SAM is required for the capping of the viral (as well as cellular) RNA (Viswanathan et al., 2020), this might further limit the production of infectious RNA. Indeed, the characterization of cellular metabolomics in response to SARS-CoV-2 infection, and the observed reduction in spermidine, at least suggested that SAM levels were reduced in infected cells (Gassen et al., 2020). However, based on the fact that the purine nucleoside inosine was capable of rescuing virus replication (Fig. 5D), we propose that the lack of purine synthesis represents the major mechanism of how MTX limits SARS-CoV-2 replication.

Using MTX against other viruses has been considered previously. As early as in 1957, it was reported that a folate antagonist was capable of protecting mice from infections with Lymphocytic Choriomeningitis Virus (LCMV; a member of the arenaviridae), while this was reverted by leucovorin (at that time still called "citrovorum factor") (Haas et al., 1957). Moreover, MTX is capable of interfering with the replication of Zika virus, another positive strand RNA virus, and a member of the flaviviridae family of viruses (Beck et al., 2019). There, again, rescue with leucovorin and adenosine indicated reduced purine synthesis as the primary mechanism of action. However, at least to our knowledge, MTX has not been broadly used as an antiviral drug. We speculate that it might be usable against other viruses with large burst sizes and corresponding demand of nucleotides as well. Of note, other flaviviridae, i.e. Dengue and West Nile Virus, were also found susceptible to treatment with MTX, whereas Sindbis and Vesicular Stomatitis Virus were not (Fischer et al., 2013). It thus remains to be determined whether MTX might also interfere with the replication of other RNA as well as DNA viruses.

With seven decades of clinical experience, MTX is one of the most established drugs whatsoever, available at low costs, making its potential use for treating COVID-19 relatively straightforward. Having said this, a number of caveats still apply. Firstly, the dose of MTX that would be needed for antiviral treatment is probably higher than the typical dose taken by patients for the purpose of long-term anti-inflammation treatment. Plasma concentrations in patients treated for rheumatoid arthritis, typically taking 7.5 mg/week for months or even years, are only around 25 nM (Hornung et al., 2008), which is unlikely to interfere with virus replication. On the other hand, when applying high-dose therapies, up to 1000 μM plasma concentrations are achievable (Comandone et al., 2005), i.e. 1000-fold more than what would be required for the antiviral effect in our study. Under such circumstances, a limiting toxicity would consist in mucositis, which is often observed when treating leukemia with high-dose MTX in a pediatric setting (den Hoed et al., 2015).

Antiviral activities of MTX would presumably require an intermediate short-term dose for a week or two. The antiviral concentration of MTX (> 1 μM) is achieved, for instance, by single intramuscular application of 50 mg MTX, which is a common procedure to induce abortions at early stages of pregnancy (Creinin and Vittinghoff, 1994). In this setting, tolerable side effects were reported, e.g. transient nausea, diarrhea, and headache (Creinin and Krohn, 1997). This comparison, on the other hand, makes it very clear that antiviral doses of MTX are contraindicated in pregnant women. While tolerable under some circumstances, the side effects of MTX might still be a major reason why it is currently not used broadly as an antiviral agent. We suggest that its clinical perspective might consist in combinations, e.g. with remdesivir, where lower concentrations of MTX appear to suffice of synergistic repression of virus replication.

A clinical study using nanoparticle-coupled MTX for treating COVID-19 was registered at clinicaltrials.gov, NCT04352465. Moreover, clinical studies using intermediate-to-high dose therapy with MTX were recently proposed for COVID-19, purely based on the rationale of immunosuppression by MTX (Frohman et al., 2020; Frohman et al., 2021). Our findings that MTX also interferes with virus replication further argues in favor of such clinical studies.

As with other antiviral drugs such as remdesivir, the timing of the therapeutic intervention appears critical. At stages where the COVID-19 symptoms are fully established, virus propagation may already have surpassed its peak. The disease is then mostly caused by excessive inflammatory responses in the lung, as well as intravasal blood coagulation. This argues in favor of early treatment with drugs that interfere with virus replication, to avoid spreading of the infection in the first place.

On the other hand, MTX may benefit COVID-19 patients not only through its direct impact on virus replication. Rather, MTX has long been known to suppress the immune response by diminishing the proliferation of B and T cells, which may reduce the pathogenesis of immune-driven lung pathology. While immune suppression would otherwise bear the risk of further virus propagation, our results strongly suggest a direct impact of MTX on viral RNA synthesis. This might allow two benefits at once, i.e. lower virus spread and lower immune reaction. Finally, MTX not only reduces the adaptive immune response, but also the inflammatory reaction, e.g. through extracellular release of adenosine (Cronstein et al., 1991) as well as by diminishing the JAK-STAT

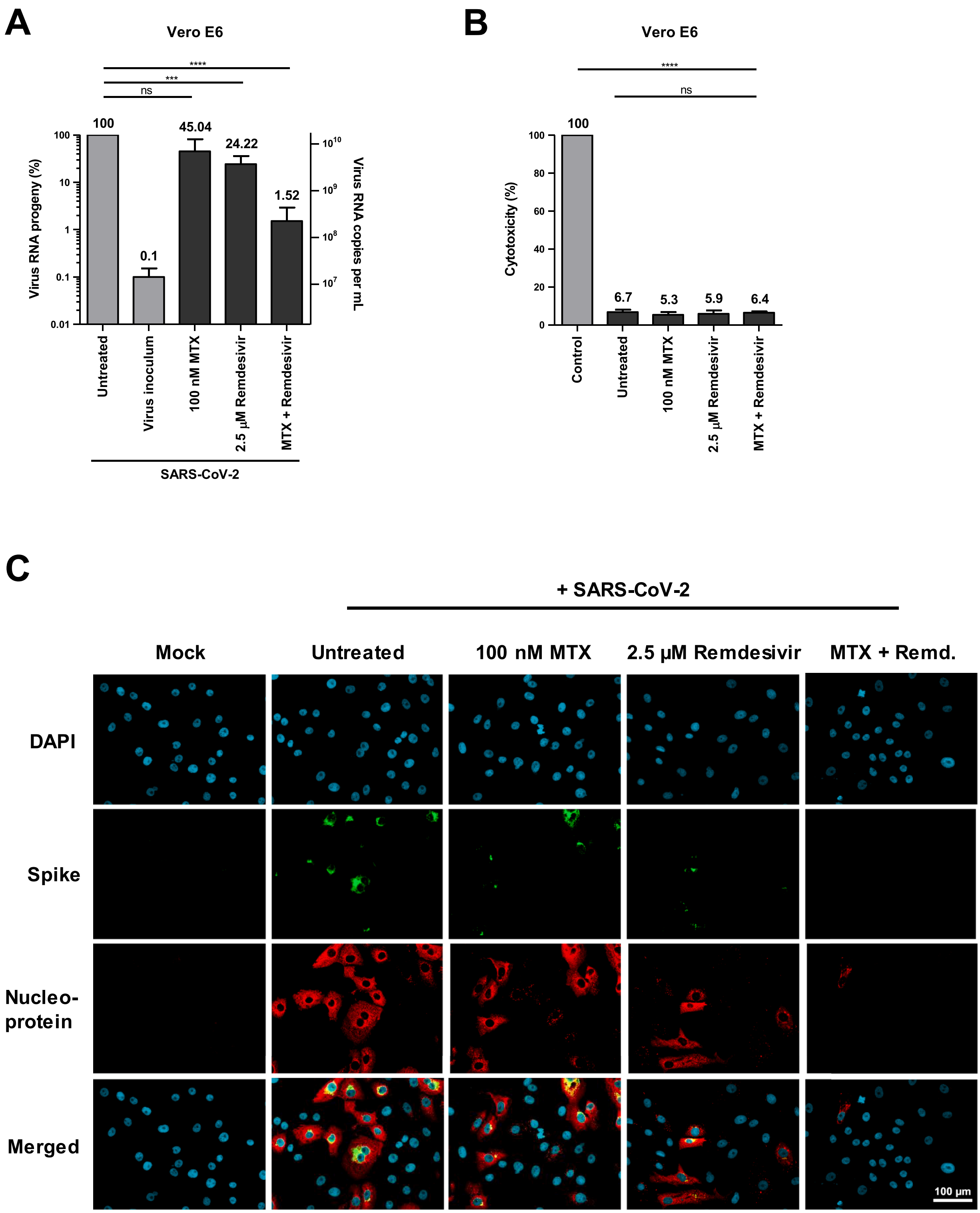

Fig. 6.. Synergism of MTX with remdesivir (A)
Remdesivir synergizes with MTX to antagonize SARS-CoV-2 replication. Vero cells were inoculated with virus as in Fig. 2, with or without MTX and remdesivir treatment 24 hrs before and during infection (mean with SD, $n = 3$). (B)
Unchanged cytotoxicity levels upon the combination treatment compared to single treatments. Vero cells were treated with MTX and/or remdesivir at the indicated concentration for 72 hrs. The LDH release into the supernatant upon disruption of the plasma membrane was measured and quantified by bioluminescence (mean with SD, $n = 3$; control = maximum LDH release). (C)
Stronger reduction of viral protein synthesis by a combination of MTX and remdesivir compared to single treatments, as determined 48 hrs p.i. by immunofluorescence analysis.

signaling pathway (Thomas et al., 2015). Indeed, the targeted JAK-STAT inhibitor baricitinib was reported to be beneficial for COVID-19 patients (Richardson et al., 2020), and combining baricitinib with MTX was suggested recently (Seif et al., 2020); furthermore, the reduction of the inflammatory response may also explain the benefits of corticosteroids in the management of COVID-19 (Li et al., 2020). So far, the use of MTX in patients with rheumatoid arthritis was at least reported to be of no detrimental effect when these patients had COVID-19 (Sanchez-Piedra et al., 2020). However, none of these studies was aiming at a direct antiviral effect of the drugs. According to the results presented here, MTX would have the additional advantage of interfering with virus replication itself.

The clinical efficacy of MTX against SARS-CoV-2 replication might be further enhanced through the combination with antivirals such as remdesivir. We propose that this combination might work in a more than additive fashion, but by a mechanistic synergism. Specifically, the reduction in available purine nucleotides might enhance the likelihood of incorporating remdesivir or similar antiviral drugs and their active metabolites into the nascent viral RNA. Such incorporation of remdesivir was shown to be required for replication fork stalling. In particular, fork progression is hindered when the enzyme is trying to incorporate the fourth nucleotide after remdesivir (Kokic et al., 2021). In any case, treatment with remdesivir and MTX might not only be tolerable but serve to potentiate antiviral efficacy.

In summary, albeit solely based on cell culture experiments so far, our study raises the possibility of using MTX, alone or in combination with remdesivir, to limit the replication of SARS-CoV-2 in patients, with the possible additional benefit of its immunosuppressive and anti-inflammatory effects to reduce the pathogenesis of COVID-19. Pending further preclinical evaluation, repurposing the established drug MTX for treating COVID-19 might be beneficial.

CRediT authorship contribution statement

Kim M. Stegmann: Conceptualization, Investigation, Methodology, Writing - review & editing. **Antje Dickmanns:** Conceptualization, Investigation, Methodology, Writing - review & editing. **Sabrina Gerber:** Data curation. **Vella Nikolova:** Investigation, Methodology. **Luisa Klemke:** Investigation, Methodology. **Valentina Manzini:** Investigation, Methodology. **Denise Schlösser:** Investigation, Methodology. **Cathrin Bierwirth:** Investigation, Methodology. **Julia Freund:** Investigation, Methodology. **Maren Sitte:** Data curation. **Raimond Lugert:** Supervision. **Gabriela Salinas:** Data curation. **Toni Luise Meister:** Investigation, Methodology. **Stephanie Pfaender:** Supervision. **Dirk Görlich:** Supervision. **Bernd Wollnik:** Data curation. **Uwe Groß:** Supervision. **Matthias Dobbelstein:** Conceptualization, Supervision, Writing - original draft.

Declaration of Competing Interest

The authors declare no conflict of interests.

Acknowledgments

We thank Stefan Pöhlmann, German Primate Center Göttingen, for helpful advice, and Marie Luise Schmidt, Institute of Virology, Charité Berlin, for SARS-CoV-2-derived RNA. Moreover, we thank Carsten Lüder and Melanie Eisele as well as the members of the Institute of Medical Microbiology for their continuous help and support in working at biosafety level 3. KMS and LK were members of the Göttingen Graduate School GGNB during this work. VN and VM were members of the IMPRS/MSc./PhD program Molecular Biology.

Supplementary materials

Supplementary material associated with this article can be found, in the online version, at doi:10.1016/j.virusres.2021.198469.

References

Beck, S., Zhu, Z., Oliveira, M.F., Smith, D.M., Rich, J.N., Bernatchez, J.A., Siqueira-Neto, J.L., 2019. Mechanism of action of methotrexate against zika virus. Viruses 11.
Fischer, M.A., Smith, J.L., Shum, D., Stein, D.A., Parkins, C., Bhinder, B., Radu, C., Hirsch, A.J., Djaballah, H., Nelson, J.A., Früh, K., 2013. Flaviviruses are sensitive to inhibition of thymidine synthesis pathways. J. Virol. 87, 9411–9419.
Estrada, A., Wright, D.L., Anderson, A.C., 2016. Antibacterial antifolates: from development through resistance to the next generation. Cold Spring Harbor perspectives in medicine 6, a028324.
Farber, S., Diamond, L.K., Mercer, R.D., Sylvester, R.F., Wolff, J.A., 1948. Temporary remissions in acute leukemia in children produced by folic acid antagonist, 4-aminopteroyl-glutamic acid. New Engl. J. Med. 238, 787–793.
Cronstein, B.N., Aune, T.M., 2020. Methotrexate and its mechanisms of action in inflammatory arthritis. Nat. Rev. Rheumatol. 16, 145–154.
Weber-Schoendorfer, C., Chambers, C., Wacker, E., Beghin, D., Bernard, N., Shechtman, S., Johnson, D., Cuppers-Maarschalkerweerd, B., Pistelli, A., Clementi, M., Winterfeld, U., Eleftheriou, G., Pupco, A., Kao, K., Malm, H., Elefant, E., Koren, G., Vial, T., Ornoy, A., Meister, R., Schaefer, C., 2014. Pregnancy outcome after methotrexate treatment for rheumatic disease prior to or during early pregnancy: a prospective multicenter cohort study. Arthritis Rheumatol. (Hoboken, N.J.) 66, 1101–1110.
den Hoed, M.A., Lopez-Lopez, E., te Winkel, M.L., Tissing, W., de Rooij, J.D., Gutierrez-Camino, A., Garcia-Orad, A., den Boer, E., Pieters, R., Pluijm, S.M., de Jonge, R., van den Heuvel-Eibrink, M.M, 2015. Genetic and metabolic determinants of methotrexate-induced mucositis in pediatric acute lymphoblastic leukemia. Pharmacogenomics J. 15, 248–254.
Payne, A.F., Binduga-Gajewska, I., Kauffman, E.B., Kramer, L.D., 2006. Quantitation of flaviviruses by fluorescent focus assay. J. Virol. Methods 134, 183–189.
Amarilla, A.A., Modhiran, N., Setoh, Y.X., Peng, N.Y.G., Sng, J.D.J., Liang, B., McMillan, C.L.D., Freney, M.E., Cheung, S.T.M., Chappell, K.J., Khromykh, A.A., Young, P.R., Watterson, D., 2021. An optimized high-throughput immuno-plaque assay for SARS-CoV-2. Front. Microbiol. 12, 625136.
McCormick, W., Mermel, L.A., 2021. The basic reproductive number and particle-to-plaque ratio: comparison of these two parameters of viral infectivity. Virol. J. 18, 92.
Corman, V.M., Landt, O., Kaiser, M., Molenkamp, R., Meijer, A., Chu, D.K., Bleicker, T., Brünink, S., Schneider, J., Schmidt, M.L., Mulders, D.G., Haagmans, B.L., van der Veer, B., van den Brink, S., Wijsman, L., Goderski, G., Romette, J.L., Ellis, J., Zambon, M., Peiris, M., Goossens, H., Reusken, C., Koopmans, M.P., Drosten, C., 2020. Detection of 2019 novel coronavirus (2019-nCoV) by real-time RT-PCR. Euro surveillance: bulletin Europeen sur les maladies transmissibles = European communicable disease. bulletin 25, 2000045.
Wu, F., Zhao, S., Yu, B., Chen, Y.M., Wang, W., Song, Z.G., Hu, Y., Tao, Z.W., Tian, J.H., Pei, Y.Y., Yuan, M.L., Zhang, Y.L., Dai, F.H., Liu, Y., Wang, Q.M., Zheng, J.J., Xu, L., Holmes, E.C., Zhang, Y.Z., 2020. A new coronavirus associated with human respiratory disease in China. Nature 579, 265–269.
Langmead, B., Salzberg, S.L., 2012. Fast gapped-read alignment with Bowtie 2. Nat. Methods 9, 357–359.
Li, H., 2011. A statistical framework for SNP calling, mutation discovery, association mapping and population genetical parameter estimation from sequencing data. Bioinformatics 27, 2987–2993.
Ramirez, F., Ryan, D.P., Gruning, B., Bhardwaj, V., Kilpert, F., Richter, A.S., Heyne, S., Dundar, F., Manke, T., 2016. deepTools2: a next generation web server for deep-sequencing data analysis. Nucleic Acids Res. 44, W160–W165.
Robinson, J.T., Thorvaldsdóttir, H., Wenger, A.M., Zehir, A., Mesirov, J.P., 2017. Variant review with the integrative genomics viewer. Cancer Res. 77, e31–e34.
Robinson, J.T., Thorvaldsdóttir, H., Winckler, W., Guttman, M., Lander, E.S., Getz, G., Mesirov, J.P., 2011. Integrative genomics viewer. Nat. Biotechnol. 29, 24–26.
Thorvaldsdóttir, H., Robinson, J.T., Mesirov, J.P., 2013. Integrative Genomics Viewer (IGV): high-performance genomics data visualization and exploration. Brief. Bioinformatics 14, 178–192.
Zhang, L., Jackson, C.B., Mou, H., Ojha, A., Rangarajan, E.S., Izard, T., Farzan, M., Choe, H., 2020. The D614G Mutation in the SARS-CoV-2 Spike Protein Reduces S1 Shedding and Increases Infectivity. bioRxiv, 2020.2006.2012.148726.
Li, Q., Wu, J., Nie, J., Zhang, L., Hao, H., Liu, S., Zhao, C., Zhang, Q., Liu, H., Nie, L., Qin, H., Wang, M., Lu, Q., Li, X., Sun, Q., Liu, J., Zhang, L., Li, X., Huang, W., Wang, Y., 2021. The impact of mutations in SARS-CoV-2 spike on viral infectivity and antigenicity. Cell.
Hoffmann, M., Kleine-Weber, H., Pöhlmann, S., 2020. A multibasic cleavage site in the spike protein of SARS-CoV-2 is essential for infection of human lung cells. Mol. Cell 78, 779–784 e775.
Ogando, N.S., Dalebout, T.J., Zevenhoven-Dobbe, J.C., Limpens, R.W., van der Meer, Y., Caly, L., Druce, J., de Vries, J.J.C., Kikkert, M., Bárcena, M., Sidorov, I., Snijder, E.J., 2020. SARS-Coronavirus-2 Replication in Vero E6 cells: Replication Kinetics, Rapid Adaptation and Cytopathology. bioRxiv. :2020.2004.2020.049924.
Liu, Z., Zheng, H., Yuan, R., Li, M., Lin, H., Peng, J., Xiong, Q., Sun, J., Li, B., Wu, J., Hulswit, R.J.G., Bowden, T.A., Rambaut, A., Loman, N., Pybus, O.G., Ke, C., Lu, J., 2020. Identification of a Common Deletion in the Spike Protein of SARS-CoV-2. bioRxiv. :2020.2003.2031.015941.
Alexandersen, S., Chamings, A., Bhatta, T.R., 2020. SARS-CoV-2 genomic and subgenomic RNAs in diagnostic samples are not an indicator of active replication. Nat. Commun. 11, 6059.
Lewin, B., 1994. Genes V. Oxford University Press, Oxford and New York.

Milo, R., Jorgensen, P., Moran, U., Weber, G., Springer, M., 2010. BioNumbers–the database of key numbers in molecular and cell biology. Nucleic Acids Res. 38, D750–D753.

Xing, J., Shankar, R., Drelich, A., Paithankar, S., Chekalin, E., Dexheimer, T., Rajasekaran, S., Tseng, C.K., Chen, B, 2020. Reversal of Infected Host Gene Expression Identifies Repurposed Drug Candidates For COVID-19. bioRxiv.

Caruso, A., Caccuri, F., Bugatti, A., Zani, A., Vanoni, M., Bonfanti, P., Cazzaniga, M.E., Perno, C.F., Messa, C., Alberghina, L., 2020. Methotrexate inhibits SARS-CoV-2 virus replication "in vitro". J. Med. Virol.

Foster, K.A., Avery, M.L., Yazdanian, M., Audus, K.L., 2000. Characterization of the Calu-3 cell line as a tool to screen pulmonary drug delivery. Int J Pharm 208, 1–11.

Tsurusawa, M., Niwa, M., Katano, N., Fujimoto, T., 1990. Methotrexate cytotoxicity as related to irreversible S phase arrest in mouse L1210 leukemia cells. Japanese J. Cancer Res. 81, 85–90.

Klein, M.E., Kovatcheva, M., Davis, L.E., Tap, W.D., Koff, A., 2018. CDK4/6 Inhibitors: the Mechanism of Action May Not Be as Simple as Once Thought. Cancer Cell 34, 9–20.

Hsieh, Y.C., Skacel, N.E., Bansal, N., Scotto, K.W., Banerjee, D., Bertino, J.R., Abali, E.E., 2009. Species-specific differences in translational regulation of dihydrofolate reductase. Mol. Pharmacol. 76, 723–733.

Paternot, S., Colleoni, B., Bisteau, X., Roger, P.P., 2014. The CDK4/CDK6 inhibitor PD0332991 paradoxically stabilizes activated cyclin D3-CDK4/6 complexes. Cell Cycle 13, 2879–2888.

Alqarni, A.M., Zeidler, M.P., 2020. How does methotrexate work? Biochem. Soc. Trans. 48, 559–567.

Bedoui, Y., Guillot, X., Selambarom, J., Guiraud, P., Giry, C., Jaffar-Bandjee, M.C., Ralandison, S., Gasque, P., 2019. Methotrexate an Old Drug with New Tricks. Int. J. Mol. Sci. 20.

Nichol, C.A., Welch, A.D., 1950. On the mechanism of action of aminopterin. In: Proceedings of the Society for Experimental Biology and Medicine. Society for Experimental Biology and Medicine. New York, N.Y., 74, pp. 403–411.

Osborn, M.J., Freeman, M., Huennekens, F.M., 1958. Inhibition of dihydrofolic reductase by aminopterin and amethopterin. In: Proceedings of the Society for Experimental Biology and Medicine. Society for Experimental Biology and Medicine. New York, N. Y., 97, pp. 429–431.

Allegra, C.J., Fine, R.L., Drake, J.C., Chabner, B.A., 1986. The effect of methotrexate on intracellular folate pools in human MCF-7 breast cancer cells. Evidence for direct inhibition of purine synthesis. J. Biol. Chem. 261, 6478–6485.

Allegra, C.J., Drake, J.C., Jolivet, J., Chabner, B.A., 1985a. Inhibition of phosphoribosylaminoimidazolecarboxamide transformylase by methotrexate and dihydrofolic acid polyglutamates. Proc. Natl. Acad. Sci. U.S.A. 82, 4881–4885.

Baggott, J.E., Vaughn, W.H., Hudson, B.B., 1986. Inhibition of 5-aminoimidazole-4-carboxamide ribotide transformylase, adenosine deaminase and 5′-adenylate deaminase by polyglutamates of methotrexate and oxidized folates and by 5-aminoimidazole-4-carboxamide riboside and ribotide. Biochem. J. 236, 193–200.

Allegra, C.J., Chabner, B.A., Drake, J.C., Lutz, R., Rodbard, D., Jolivet, J., 1985b. Enhanced inhibition of thymidylate synthase by methotrexate polyglutamates. J. Biol. Chem. 260, 9720–9726.

Borsa, J., Whitmore, G.F., 1969. Studies relating to the mode of action of methotrexate. 3. Inhibition of thymidylate synthetase in tissue culture cells and in cell-free systems. Mol. Pharmacol. 5, 318–332.

Chu, E., Drake, J.C., Boarman, D., Baram, J., Allegra, C.J, 1990. Mechanism of thymidylate synthase inhibition by methotrexate in human neoplastic cell lines and normal human myeloid progenitor cells. J. Biol. Chem. 265, 8470–8478.

Chabner, B.A., Allegra, C.J., Curt, G.A., Clendeninn, N.J., Baram, J., Koizumi, S., Drake, J.C., Jolivet, J., 1985. Polyglutamation of methotrexate. Is methotrexate a prodrug? J. Clin. Invest. 76, 907–912.

Chan, E.S., Cronstein, B.N., 2010. Methotrexate–how does it really work? Nat Rev Rheumatol 6, 175–178.

Kozminski, P., Halik, P.K., Chesori, R., Gniazdowska, E., 2020. Overview of dual-acting drug methotrexate in different neurological diseases, autoimmune pathologies and cancers. Int J Mol Sci 21.

Wang, Y., Zhang, D., Du, G., Du, R., Zhao, J., Jin, Y., Fu, S., Gao, L., Cheng, Z., Lu, Q., Hu, Y., Luo, G., Wang, K., Lu, Y., Li, H., Wang, S., Ruan, S., Yang, C., Mei, C., Wang, Y., Ding, D., Wu, F., Tang, X., Ye, X., Ye, Y., Liu, B., Yang, J., Yin, W., Wang, A., Fan, G., Zhou, F., Liu, Z., Gu, X., Xu, J., Shang, L., Zhang, Y., Cao, L., Guo, T., Wan, Y., Qin, H., Jiang, Y., Jaki, T., Hayden, F.G., Horby, P.W., Cao, B., Wang, C., 2020. Remdesivir in adults with severe COVID-19: a randomised, double-blind, placebo-controlled, multicentre trial. Lancet 395, 1569–1578.

Beigel, J.H., Tomashek, K.M., Dodd, L.E., Mehta, A.K., Zingman, B.S., Kalil, A.C., Hohmann, E., Chu, H.Y., Luetkemeyer, A., Kline, S., Lopez de Castilla, D., Finberg, R. W., Dierberg, K., Tapson, V., Hsieh, L., Patterson, T.F., Paredes, R., Sweeney, D.A., Short, W.R., Touloumi, G., Lye, D.C., Ohmagari, N., Oh, M.D., Ruiz-Palacios, G.M., Benfield, T., Fatkenheuer, G., Kortepeter, M.G., Atmar, R.L., Creech, C.B., Lundgren, J., Babiker, A.G., Pett, S., Neaton, J.D., Burgess, T.H., Bonnett, T., Green, M., Makowski, M., Osinusi, A., Nayak, S., Lane, H.C., Members, A.-.S.G., 2020. Remdesivir for the Treatment of Covid-19 - Final Report. New Engl. J. Med. 383, 1813–1826.

Spinner, C.D., Gottlieb, R.L., Criner, G.J., Arribas López, J.R., Cattelan, A.M., Soriano Viladomiu, A., Ogbuagu, O., Malhotra, P., Mullane, K.M., Castagna, A., Chai, L.Y.A., Roestenberg, M., Tsang, O.T.Y., Bernasconi, E., Le Turnier, P., Chang, S.C., SenGupta, D., Hyland, R.H., Osinusi, A.O., Cao, H., Blair, C., Wang, H., Gaggar, A., Brainard, D.M., McPhail, M.J., Bhagani, S., Ahn, M.Y., Sanyal, A.J., Huhn, G., Marty, F.M, 2020. Effect of Remdesivir vs Standard Care on Clinical Status at 11 Days in Patients With Moderate COVID-19: a Randomized Clinical Trial. JAMA 324, 1048–1057.

Zhang, Y., Guo, R., Kim, S.H., Shah, H., Zhang, S., Liang, J.H., Fang, Y., Gentili, M., Leary, C.N.O., Elledge, S.J., Hung, D.T., Mootha, V.K., Gewurz, B.E., 2021. SARS-CoV-2 hijacks folate and one-carbon metabolism for viral replication. Nat. Commun. 12, 1676.

Allison, A.C., Eugui, E.M., 1996. Purine metabolism and immunosuppressive effects of mycophenolate mofetil (MMF). Clin. Transplant. 10, 77–84.

Kato, F., Matsuyama, S., Kawase, M., Hishiki, T., Katoh, H., Takeda, M., 2020. Antiviral activities of mycophenolic acid and IMD-0354 against SARS-CoV-2. Microbiol. Immunol. 64, 635–639.

Madak, J.T., Bankhead 3rd, A., Cuthbertson, C.R., Showalter, H.D., Neamati, N., 2019. Revisiting the role of dihydroorotate dehydrogenase as a therapeutic target for cancer. Pharmacol. Ther. 195, 111–131.

Luban, J., Sattler, R.A., Mühlberger, E., Graci, J.D., Cao, L., Weetall, M., Trotta, C., Colacino, J.M., Bavari, S., Strambio-De-Castillia, C., Suder, E.L., Wang, Y., Soloveva, V., Cintron-Lue, K., Naryshkin, N.A., Pykett, M., Welch, E.M., O'Keefe, K., Kong, R., Goodwin, E., Jacobson, A., Paessler, S., Peltz, S.W., 2021. The DHODH inhibitor PTC299 arrests SARS-CoV-2 replication and suppresses induction of inflammatory cytokines. Virus Res. 292, 198246.

Coelho, A.R., Oliveira, P.J., 2020. Dihydroorotate dehydrogenase inhibitors in SARS-CoV-2 infection. Eur. J. Clin. Invest. 50, e13366.

Viswanathan, T., Arya, S., Chan, S.-.H., Qi, S., Dai, N., Hromas, R.A., Park, J.-.G., Oladunni, F., Martinez-Sobrido, L., Gupta, Y.K., 2020. Structural Basis of RNA Cap Modification By SARS-CoV-2 Coronavirus. bioRxiv. :2020.2004.2026.061705.

Gassen, N.C., Papies, J., Bajaj, T., Dethloff, F., Emanuel, J., Weckmann, K., Heinz, D.E., Heinemann, N., Lennarz, M., Richter, A., Niemeyer, D., Corman, V.M., Giavalisco, P., Drosten, C., Müller, M.A., 2020. Analysis of SARS-CoV-2-Controlled Autophagy Reveals Spermidine, MK-2206, and Niclosamide As Putative Antiviral Therapeutics. bioRxiv. :2020.2004.2015.997254.

Haas, V.H., Stewart, S.E., Briggs, G.M., 1957. Folic acid deficiency and the sparing of mice infected with the virus of lymphocytic choriomeningitis. Virology 3, 15–21.

Hornung, N., Ellingsen, T., Attermann, J., Stengaard-Pedersen, K., Poulsen, J.H., 2008. Patients with rheumatoid arthritis treated with methotrexate (MTX): concentrations of steady-state erythrocyte MTX correlate to plasma concentrations and clinical efficacy. J. Rheumatol. 35, 1709–1715.

Comandone, A., Passera, R., Boglione, A., Tagini, V., Ferrari, S., Cattel, L., 2005. High dose methotrexate in adult patients with osteosarcoma: clinical and pharmacokinetic results. Acta Oncol (Madr) 44, 406–411.

Creinin, M.D., Vittinghoff, E., 1994. Methotrexate and misoprostol vs misoprostol alone for early abortion. A randomized controlled trial. JAMA 272, 1190–1195.

Creinin, M.D., Krohn, M.A., 1997. Methotrexate pharmacokinetics and effects in women receiving methotrexate 50mg and 60mg per square meter for early abortion. Am. J. Obstet. Gynecol. 177, 1444–1449.

Frohman, E.M., Villemarette-Pittman, N.R., Cruz, R.A., Longmuir, R., Rowe, V., Rowe, E. S., Varkey, T.C., Steinman, L., Zamvil, S.S., Frohman, T.C., 2020. Part II. high-dose methotrexate with leucovorin rescue for severe COVID-19: an immune stabilization strategy for SARS-CoV-2 induced 'PANIC' attack. J. Neurol. Sci., 116935

Frohman, E.M., Villemarette-Pittman, N.R., Melamed, E., Cruz, R.A., Longmuir, R., Varkey, T.C., Steinman, L., Zamvil, S.S., Frohman, T.C., 2021. 2020. Part I. SARS-CoV-2 triggered 'PANIC' attack in severe COVID-19. J. Neurol. Sci., 116936

Cronstein, B.N., Eberle, M.A., Gruber, H.E., Levin, R.I., 1991. Methotrexate inhibits neutrophil function by stimulating adenosine release from connective tissue cells. Proc. Natl. Acad. Sci. U.S.A. 88, 2441–2445.

Thomas, S., Fisher, K.H., Snowden, J.A., Danson, S.J., Brown, S., Zeidler, M.P., 2015. Methotrexate Is a JAK/STAT Pathway Inhibitor. PLoS ONE 10, e0130078.

Richardson, P., Griffin, I., Tucker, C., Smith, D., Oechsle, O., Phelan, A., Stebbing, J., 2020. Baricitinib as potential treatment for 2019-nCoV acute respiratory disease. Lancet 395, e30–e31.

Seif, F., Aazami, H., Khoshmirsafa, M., Kamali, M., Mohsenzadegan, M., Pornour, M., Mansouri, D., 2020. JAK Inhibition as a New Treatment Strategy for Patients with COVID-19. Int. Arch. Allergy Immunol. 181, 467–475.

Li, H., Chen, C., Hu, F., Wang, J., Zhao, Q., Gale, R.P., Liang, Y., 2020. Impact of corticosteroid therapy on outcomes of persons with SARS-CoV-2, SARS-CoV, or MERS-CoV infection: a systematic review and meta-analysis. Leukemia 34, 1503–1511.

Sanchez-Piedra, C., Diaz-Torne, C., Manero, J., Pego-Reigosa, J.M., Rua-Figueroa, I., Gonzalez-Gay, M.A., Gomez-Reino, J., Alvaro-Gracia, J.M., Bs, group, 2020. Clinical features and outcomes of COVID-19 in patients with rheumatic diseases treated with biological and synthetic targeted therapies. Ann. Rheum. Dis. 79, 988–990.

Kokic, G., Hillen, H.S., Tegunov, D., Dienemann, C., Seitz, F., Schmitzova, J., Farnung, L., Siewert, A., Höbartner, C., Cramer, P., 2021. Mechanism of SARS-CoV-2 polymerase stalling by remdesivir. Nat. Commun. 12, 279.